

ARTICLE

<https://doi.org/10.1038/s41467-019-09416-2>

OPEN

Specialized dendritic cells induce tumor-promoting IL-10⁺IL-17⁺ FoxP3^{neg} regulatory CD4⁺ T cells in pancreatic carcinoma

Rocky M. Barilla¹, Brian Diskin¹, Raul Caso Caso¹, Ki Buom Lee¹, Navyatha Mohan¹, Chandan Buttar¹, Salma Adam¹, Zennur Sekendiz¹, Junjie Wang¹, Ruben D. Salas¹, Marcelo F. Cassini¹, Jason Karlen¹, Belen Sundberg¹, Hashem Akbar¹, Dmitry Levchenko¹, Inderdeep Gakhal¹, Johana Gutierrez¹, Wei Wang¹, Mautin Hundeyin¹, Alejandro Torres-Hernandez¹, Joshua Leinwand¹, Emma Kurz¹, Juan A. Kochen Rossi¹, Ankita Mishra¹, Miguel Liria¹, Gustavo Sanchez¹, Jyoti Panta², P'ng Loke², Berk Aykut¹ & George Miller^{1,3}

The drivers and the specification of CD4⁺ T cell differentiation in the tumor microenvironment and their contributions to tumor immunity or tolerance are incompletely understood. Using models of pancreatic ductal adenocarcinoma (PDA), we show that a distinct subset of tumor-infiltrating dendritic cells (DC) promotes PDA growth by directing a unique T_H-program. Specifically, CD11b⁺CD103⁻ DC predominate in PDA, express high IL-23 and TGF- β , and induce FoxP3^{neg} tumor-promoting IL-10⁺IL-17⁺IFN γ ⁺ regulatory CD4⁺ T cells. The balance between this distinctive T_H program and canonical FoxP3⁺ T_{REGS} is unaffected by pattern recognition receptor ligation and is modulated by DC expression of retinoic acid. This T_H-signature is mimicked in human PDA where it is associated with immune-tolerance and diminished patient survival. Our data suggest that CD11b⁺CD103⁻ DC promote CD4⁺ T cell tolerance in PDA which may underscore its resistance to immunotherapy.

¹S. Arthur Localio Laboratory, Department of Surgery, New York University School of Medicine, 550 First Avenue, New York, NY 10016, USA. ²Department of Microbiology, New York University School of Medicine, 550 First Avenue, New York, NY 10016, USA. ³Department of Cell Biology, New York University School of Medicine, 550 First Avenue, New York, NY 10016, USA. These authors contributed equally: Rocky M. Barilla, Brian Diskin. Correspondence and requests for materials should be addressed to G.M. (email: george.miller@nyumc.org)

Autoimmunity denotes inflammatory responses directed against an organism's own cells and tissues, and is driven by the systematic breakdown of the regulatory checkpoints governing cellular inhibition and self-tolerance. Peripheral tolerance can be mediated on a cellular level through the effector functions of distinct subsets of CD4⁺ T cells, including FoxP3⁺ T regulatory (T_{REG}) cells and FoxP3^{neg} type-1 regulatory (Tr1) cells, or on a cell-intrinsic level through the upregulation of inhibitory receptors^{1–3}. Since failure of these inhibitory processes can potentiate autoimmune responses against host antigens, it is not surprising that therapies targeting mechanisms of immune tolerance are being intensely investigated as potential treatments for cancer. Illustrating this is the recent advancement in checkpoint blockade and T-cell engineering, which has spurred a renaissance in cancer immunotherapy through approaches that override regulatory circuits to promote antitumor immunity⁴. Nonetheless, there are particular cancers, including pancreatic ductal adenocarcinoma (PDA), which respond very poorly to checkpoint blockade and adoptive T-cell therapy⁵. This may indicate the presence of a highly immunosuppressive tumor micro-environment (TME) that supports distinct, yet redundant, T-cell inhibitory programs. Alternatively, poor responses to immunotherapy may signify an obstruction in the stepwise process of T-cell priming by dendritic cells (DCs). Recent studies have described specialized subsets of TME-infiltrating antigen-presenting cells (APCs) distinguished by their unique abilities to prime, educate, and expand tumor-specific effector CD8⁺ T cells⁶. Antitumor cytotoxic T-cell responses are additionally influenced by fibrosis, infiltrating innate immune cells, and a number of TME-derived factors, all promoting immune tolerance through a variety of mechanisms^{7–9}. Further, because of the complex repertoires of tolerogenic programs in select cancer subtypes, targeting CD8⁺ T cells alone may be insufficient to mount an adaptive immune response against specific tumors. As a result, ancillary methods of intervention may be required to consider T-cell-targeted therapy as a viable treatment modality for specific cancers.

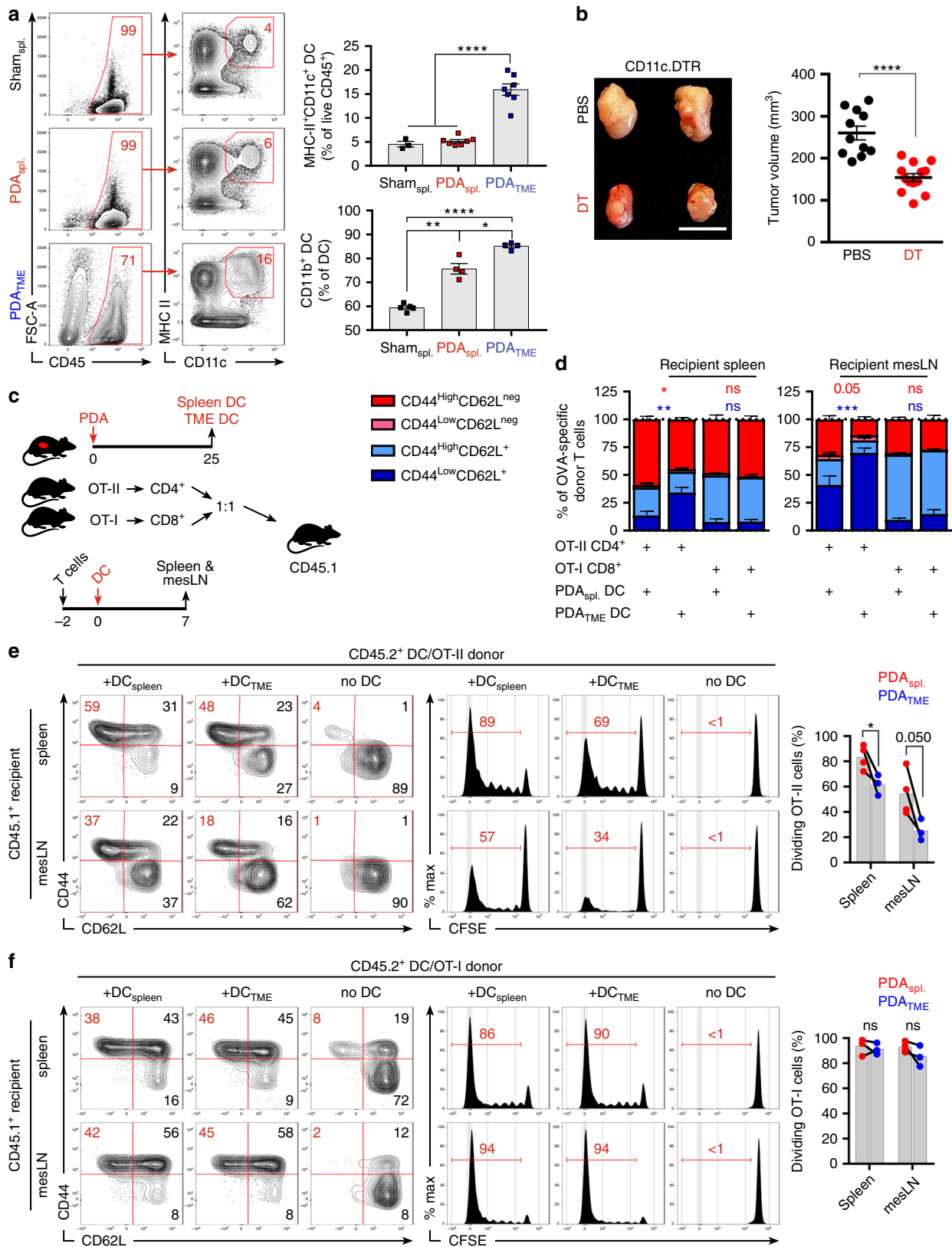
Several autoimmune diseases (e.g., Crohn's disease and psoriasis) have been linked to the imbalance of pathologic T_H17 cells and tolerogenic T_{REGS}^{10–12}. In these diseases, the ultimate fate of CD4⁺ T-helper (T_H) cell differentiation is attributed, at least in part, to the influence of DC from the site of inflammation¹³. While CD8⁺ T-cell priming by TME-infiltrating DC has been studied, we still have a limited understanding of (i) how tumor-infiltrating DCs direct CD4⁺ T_H-cell differentiation and (ii) the functional roles differentiated T_H effector cells play in tumor progression. Furthermore, there is a lack of consensus on the role of TME-infiltrating T_H17 cells in tumor progression, which may point to the functional complexity of this subset^{14–16}. This discordance may stem from the de facto sufficiency of cytokine expression for classifying T-cell subsets without detailed functional analyses. The existence of both tolerogenic IL-17A⁺ T_{REGS} and immunogenic IL-17⁺ T_H17 cells suggests that IL-17⁺ T_H cells may represent several functionally distinct subsets¹⁷. As cytotoxic CD8⁺ effector function is highly dependent on CD4⁺ T-cell cooperation, exploration of cellular and biochemical drivers T_H-cell differentiation may hold promise for making resistant cancers more immunogenic. As such, we investigated the effect of DC education on T_H-cell programming and immune tolerance in the PDA TME.

Results

PDA-infiltrating DC direct CD4⁺ T-cell differentiation and promote disease progression. Along with others, we have shown that CD4⁺ T cells are ineffective at generating antitumor

immunity in PDA^{18–20}. We postulated that select DC subsets within the TME entrain CD4⁺ T cells towards a tolerogenic phenotype. Approximately 15% of CD45⁺ leukocytes infiltrating primary PDA tumors in mice were CD11c⁺MHCII⁺ (PDA_{TME} DC) (Fig. 1a). The percentage of DC in the spleens of PDA-bearing mice (PDA_{spl}) was similar to control spleen (sham_{spl}); however, PDA_{spl} DC contained a greater CD11b⁺ fraction (Fig. 1a). To investigate the influence of DC on tumor progression, we utilized CD11c.DTR bone marrow chimeric mice, which allowed for serial depletion of DC after PDA establishment (Supplementary Figure 1A–B). Macrophage and T-cell infiltration and macrophage phenotype were unchanged after DC depletion (Supplementary Figure 1C, D). DC depletion resulted in marked tumor protection (Fig. 1b). DC depletion was similarly protective in a PDA liver metastases model (Fig. S1E). We hypothesized that PDA_{TME} DC facilitate tumor progression by inducing tolerogenic CD4⁺ or CD8⁺ T-cell differentiation. To test this, we performed an in vivo CD4⁺ and CD8⁺ T-cell expansion assay by adoptively transferring carboxyfluorescein *N*-succinimidyl ester (CFSE)-labeled antigen-restricted CD4⁺ and CD8⁺ T cells from OT-II and OT-I donors, respectively, into congenic CD45.1 mice followed by the transfer of Ova-pulsed DC from either the spleen or TME (Fig. 1c). Splenic and nodal CD45.2⁺CD4⁺ T cells in hosts receiving antigen-pulsed PDA_{TME} DC exhibited diminished activation—evidenced by a smaller CD44^{high}CD62L^{neg} population—and a lower proliferative response than in mice primed by Ova-pulsed splenic DC (Figs. 1d, e). In addition, while interferon- γ (IFN γ) was similarly expressed by antigen-restricted CD4⁺ T cells in mice transferred with spleen or TME-derived DC, the expression of interleukin (IL)-17A was significantly greater in CD4⁺ T cells primed by TME-derived DC (Supplementary Figure 1F). These observations were not a result of DC immaturity or inability to capture antigen as PDA_{TME} DC expressed significantly higher CD86, ICOS-ligand (ICOSL), CCR7, and MHCII and captured antigen more avidly than splenic DC subsets (Supplementary Figure 1G and H). The elevated expression of IL-17A in antigen-restricted CD4⁺ T cells primed by PDA_{TME} DC paralleled the phenotype of CD4⁺ T cells in situ in PDA, which expressed greater IL-17A than splenic CD4⁺ T cells in PDA-bearing mice (Supplementary Figure 1I). To determine whether CD4⁺ T-cell expression of IL-17 in situ in PDA was DC dependent, we depleted DC in PDA-bearing CD11c.DTR bone marrow chimeric mice. Ablation of DC mitigated CD4⁺ T-cell expression of IL-17 and retinoic acid receptor-related orphan receptor gamma t (ROR γ t) (Supplementary Figure 1J). Ablation of DC similarly reduced CD4⁺ T-cell expression of IL-17 and ROR γ t in the PDA liver metastases model (Supplementary Figure 1K). In contrast to the differential effects of PDA_{TME} DC on CD4⁺ T-cell differentiation, the proliferation and activation of antigen-restricted CD8⁺ T cells did not differ between hosts primed with PDA_{TME} DC versus splenic DC (Figs. 1d, f), suggesting distinct influences of PDA_{TME} DC on CD4⁺ T-cell differentiation. To definitively determine whether the tumor-protective effects of DC depletion were CD4⁺ T-cell dependent, we ablated DC in PDA-bearing hosts in the context of CD4⁺ T-cell depletion. Absence of CD4⁺ T cells negated the tumor-protective effect of DC depletion, suggesting that the protection afforded by DC ablation was CD4⁺ T-cell dependent (Supplementary Figure 2A). By contrast, DC depletion offered residual protective effects in absence of CD8⁺ T cells (data not shown). This led us to believe that PDA_{TME} DC may constrain CD4⁺ T-cell-driven antitumor responses and motivated us to further investigate their interactions.

PDA_{TME} DC induce a distinct CD4⁺ T-cell program. To determine how PDA entrainment affects DC capacity for T_H-cell



differentiation, we co-cultured Ova-pulsed PDA_{TME} DC and controls with Ova-restricted CD4⁺ T cells. Consistent with our in vivo data, PDA_{TME} DC possessed enhanced capacity for the induction of IL-17 as evidenced by increased generation of IL-17A⁺TNFα⁺ and IL-17A⁺IFNγ⁺ CD4⁺ T cells (Figs. 2a, b; Supplementary Figure 2B). By contrast, splenic DC groups were

not efficient at inducing IL-17 expression in CD4⁺ T cells. The T_H phenotype induced by PDA_{TME} DC was verified through the assessment of secreted cytokines, which exhibited the highest concentrations of T_H17-associated cytokines IL-17A and IL-6, and lowest concentrations of IL-2 compared with splenic DC-CD4⁺ T-cell co-cultures (Fig. 2c; Supplementary Figure 2C).

Fig. 1 Distinct pancreatic ductal adenocarcinoma (PDA)-infiltrating dendritic cell (DC) promote tumor progression and regulate CD4⁺ T-cell differentiation. **a** CD45⁺ cells from the spleen or tumor of orthotopic PDA-bearing mice or from the spleen of control mice were gated using flow cytometry and tested for co-expression of CD11c and MHCII. CD11c⁺MHCII⁺ cells were then sub-gated and tested for expression of CD11b. Representative contour plots and quantitative data are shown. This experiment was repeated >5 times. **b** WT mice were made chimeric using bone marrow from CD11c-DTR mice. Cohorts were challenged with orthotopic PDA 7 weeks later. On day 12, mice began serial treatment with diphtheria toxin (DT) or phosphate-buffered saline (PBS) before sacrifice on day 25. Representative gross images of tumors and quantitative analysis of tumor volume are shown. This experiment had similar results for >5 times (scale bars = 1 μm). **c-f** PDA_{TME} DC were harvested on day 25 from tumor-bearing mice, loaded with either Ova₂₂₃₋₃₃₉ or Ova₂₅₇₋₂₆₄ peptide and administered in equal number i.p. to CD45.1 mice that had been transferred i.v. 2 days prior with equal numbers of CFSE-labeled OT-I and OT-II T cells. Parallel experiments were performed using PDA_{spl} DC. On day 7 after either PDA_{TME} or PDA_{spl} DC/Ova administration, spleen and mesenteric lymph nodes (LNs) were harvested and CD45.2⁺ CD4⁺ and CD8⁺ T cells tested for co-expression of CD44 and CD62L and dilution of CFSE. **c** A schematic of the experimental regimen is depicted. **d** Quantitative results and **e** representative flow cytometry data for CD4⁺ T cells and **f** CD8⁺ T cells are shown. This experiment was repeated twice (**p* < 0.05, ***p* < 0.01, ****p* < 0.001, *****p* < 0.0001, *t*-test), SEM

CD4⁺ T-cell expression of IL-10 was also differentially induced by PDA_{TME} DC (Supplementary Figure 2C). Consistent with the cytokine profile of PDA_{TME} DC-entrained CD4⁺ T cells, Ova-pulsed PDA_{TME} DC induced more RORγt⁺ and FoxP3⁺ Ova-restricted CD4⁺ T cells but fewer T-bet⁺ CD4⁺ cells than did control DC populations (Supplementary Figure 2D and E). We confirmed these results in an alternate model of T-cell activation as PDA_{TME} DC promoted the secretion of greater IL-17A and IL-6, but less IL-2, in mixed lymphocyte reactions (MLRs) with allogeneic CD4⁺ T cells (Supplementary Figure 2F). Similarly, IL-17-rich cytokine profiles were observed in antigen-restricted CD4⁺ T cells co-cultured with antigen-pulsed PDA_{TME} DC that were harvested from both autochthonous *P48^{Cre};Kras^{G12D}* (KC) and *Pdx1^{Cre};Kras^{G12D};Tp53^{R172H}* (KPC) mouse PDA tumors, suggesting these observations are not specific to the orthotopic PDA model (Supplementary Figure 2G, H).

Because CD4⁺ T-cell differentiation can be driven by secreted inflammatory mediators, we examined the cytokines produced by PDA_{TME} DC. Purified PDA_{TME} DC produced markedly elevated TNFα, IL-6, and IL-10 in culture compared with splenic DC from tumor-bearing hosts (Fig. 2d). Further, intracellular cytokine analysis suggested that PDA_{TME} DC expressed elevated levels of additional T_H17- and T_{REG}-inducing cytokines, including IL-23 and transforming growth factor β (TGF-β) (Fig. 2e, f). Notably, IL-6 expression by PDA_{TME} DC occurred exclusively in TGF-β⁺ cells (Fig. 2f). Thus, PDA_{TME} DCs influence naive T cells to differentiate into IL-17A⁺IFNγ⁺ CD4⁺ T cells and are phenotypically equipped with the cytokine requirements for T_H17-differentiation.

CD4⁺ T-cell differentiation by PDA_{TME} DC is independent of TLR2 and Dectin-1 but is modulated by retinoic acid signaling.

As DC cytokine production and capacity for T-cell polarization may be dependent on specific environmental cues, we interrogated PDA-associated DC subsets for expression of innate immune receptors linked to T_H17 or T_{REG} induction. PDA_{TME} DC expressed elevated Dectin-1, CD206, and TLR2 cells compared with splenic DC populations, with the vast majority of Dectin-1⁺ PDA_{TME} DC co-expressing TLR2 and ICOSL (Supplementary Figure 3A–C). We have recently shown that the PDA TME is rife with Dectin-1 and TLR2 ligands^{21,22}. Consistent with their higher Dectin-1 and TLR2 expression, PDA_{TME} DC secreted more TNFα, IL-6, and IL-10 than splenic DC in the presence of TLR2 (Pam₂CSK₄) and/or Dectin-1 (zymosan-depleted) ligands (Supplementary Figure 3D). To determine the influence of TLR2 and Dectin-1 signaling in PDA_{TME} DC modulation of CD4⁺ T-cell differentiation, we co-cultured Ova-restricted CD4⁺ T cells with Ova-pulsed PDA_{TME} DC in the presence or absence of zymosan-depleted or Pam₂CSK₄. Surprisingly, neither of these pattern recognition receptor ligands enhanced IL-17A expression

in PDA_{TME} DC—CD4⁺ T-cell co-cultures (Supplementary Figure 3E). However, both Dectin-1 and TLR2 ligation in PDA_{TME} DC amplified their capacity to promote expression of IL-10, IL-6, IFN-γ, and TNFα in CD4⁺ T cells (Supplementary Figure 3E).

Activation of TLR2 and Dectin-1 can modulate tolerogenic or immunogenic T-cell responses by generating retinoic acid (RA) production in DC^{23,24}. RA promotes the generation of FoxP3⁺ T_{REG}s, while mitigating T_H17 differentiation¹². Of note, PDA_{TME} DC were the principal producers of RA among CD45⁺ tumor-infiltrating leukocytes and expressed higher RA than spleen DC (Supplementary Figure 4A and B). CD45^{neg} cells in primary PDA tumors, as well as in vitro cultured PDA tumor cells, also produced high RA (Supplementary Figure 4A–C). As T cells infiltrating PDA are presumably exposed to RA produced by both DC and the transformed epithelial cells, we investigated PDA_{TME} DC induction of T_H differentiation in the presence of exogenous *all-trans* RA (ATRA) or LE135, a RA receptor-α/β inhibitor. As expected, ATRA attenuated IL-17A and IFNγ secretion, upregulated IL-2 expression, and reduced ICOS surface expression on CD4⁺ T cells consistent with a phenotype of impaired IL-17⁺IFNγ⁺ cellular differentiation (Supplementary Figure 4D and E). By contrast, whereas LE135 did not have significant effects on IL-17 and IFNγ expression, it diminished FoxP3 expression on CD4⁺ T cells (Supplementary Figure 4F), suggesting a critical role of RA signaling in determining terminal T_H-cell differentiation by PDA_{TME} DC.

Distinct populations of PDA_{TME} DC have the requisite potential for inducing T_H17 or T_{REG} differentiation.

Of note, tumor-associated macrophages did not express high CD11c in PDA (Fig. S4G and H). Divergent T-cell fates are directed by specific subpopulations of DC, which can be identified by the differential expression of CD11b and CD103 (Fig. 3a)^{13,25}. The majority of DC in the PDA TME were CD103[−]CD11b⁺, followed by CD103⁺CD11b⁺, and CD103⁺CD11b[−], respectively (Fig. 3b). Re-examination of DC cytokine production in the context of these subsets revealed that CD103[−]CD11b⁺ DC_{TME} produced greater IL-23p19, IL-6, and TGF-β, compared with other DC_{TME} populations (Fig. 3c). Similarly, CD103[−]CD11b⁺ DC_{TME} exceeded the other DC_{TME} subsets in co-expression of IL-6 and TGF-β (Fig. 3d). However, CD103[−]CD11b⁺ DC_{TME} produced lower RA than the CD103⁺CD11b⁺ DC_{TME} population (Fig. 3e).

CD103[−]CD11b⁺ PDA_{TME} DC induce the differentiation of immune-suppressive tumor-promoting FoxP3^{neg} CD4⁺ T cells.

To test whether the specific subsets of PDA_{TME} DC differentially influence CD4⁺ T-cell programming, we co-cultured the Ova-pulsed PDA_{TME} DC subsets with antigen-restricted CD4⁺ T cells. Both CD103[−]CD11b⁺ and CD103⁺CD11b⁺ DC_{TME} populations induced greater T-cell proliferation (Fig. 4a) and CD103[−]CD11b⁺

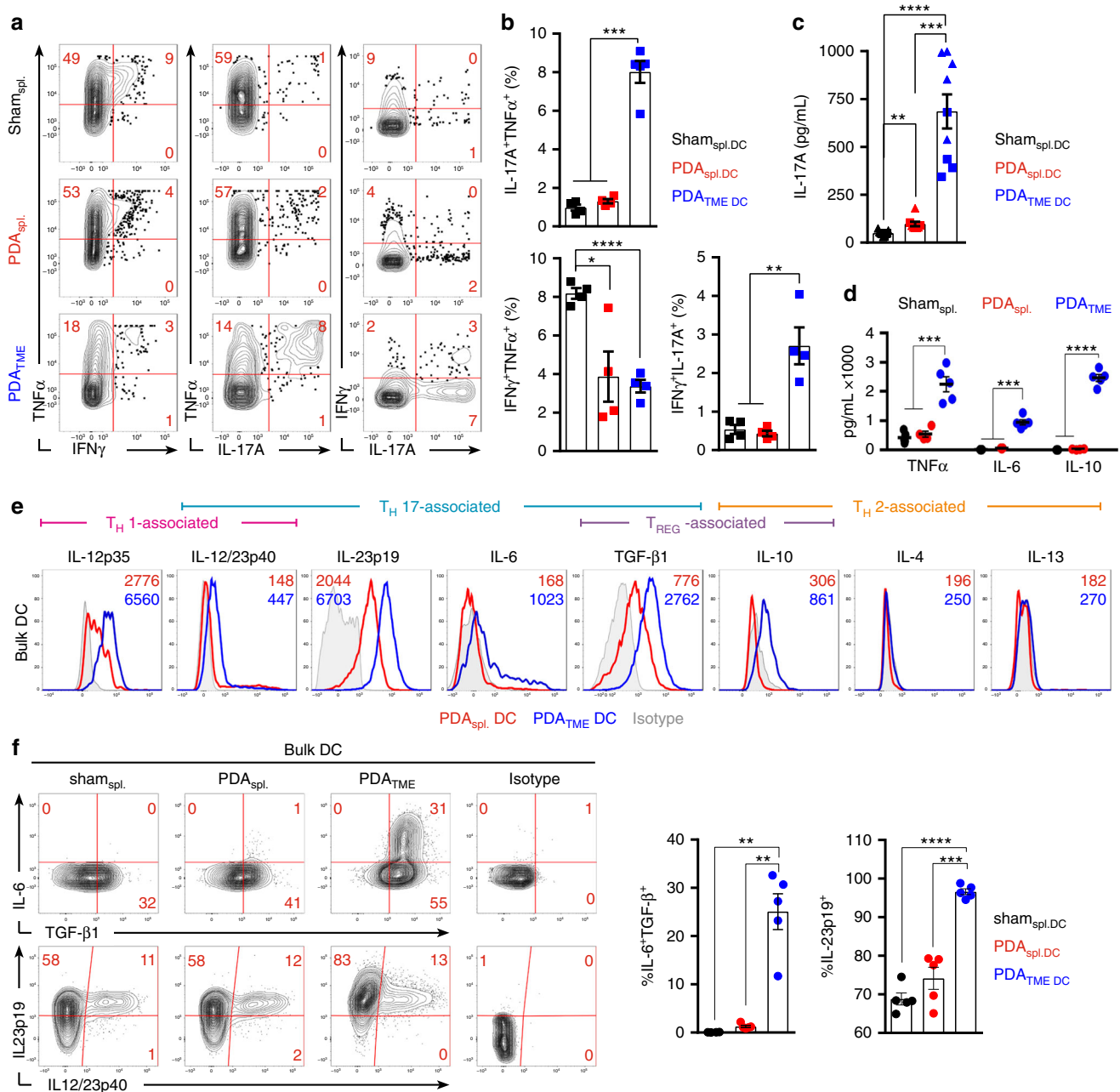


Fig. 2 PDA_{TME} dendritic cell (DC) exhibit a unique cytokine profile and promote IL-17 expression in naive CD4⁺ T cells. **a–c** Ova_{323–339} peptide-pulsed PDA_{TME} DC and splenic DC controls were co-cultured with Ova-restricted CD4⁺ T cells at a 1:5 ratio for 5 days. Representative **(a)** and quantitative **(b)** intracellular cytokine expression in the CD4⁺ T cells are shown. Data are representative of five independent experiments using 3–6 mice per arm, showing similar results. **c** Concentration of IL-17A in the supernatants of co-cultures were determined. Squares and triangles denote data points from individual mice, pooled from two independent experiments. **d** PDA_{TME} DC and splenic DC controls were plated at a density of 5 × 10⁵ cells/ml without re-stimulation and supernatant cytokine concentrations were determined after 36 h in a cytometric bead array. Data are representative of experiments repeated >3 times. **e** Orthotopic pancreatic ductal adenocarcinoma (PDA) tumors and spleens were harvested from mice on day 25 post-implantation. Intracellular flow cytometric analysis of DC cytokine expression after 12 h of re-stimulation with LPS (1 μg/ml) is shown. Representative histograms are shown. Numbers represent median fluorescence indices (MFI). Data are representative of experiments repeated >3 times. **f** The frequency of IL-6, TGF-β1 and IL23p19, IL12/23p40 co-expression in PDA_{TME} DC and splenic DC controls were tested. Representative contour plots and quantitative data are shown (n = 5 per group). This experiment was repeated three times (*p < 0.05, **p < 0.01, ***p < 0.001, ****p < 0.0001, t-test), SEM

DC_{TME} induced higher ICOS expression than CD103⁺CD11b[−] DC_{TME} (Fig. 4b). Further, the CD103[−]CD11b⁺ and CD103⁺CD11b⁺ DC_{TME} populations induced the greatest fraction of IL-17A⁺ and IL-17F⁺ CD4⁺ T cells, including a substantial IL-17A⁺IFNγ⁺ population (Fig. 4c and Supplementary Figure 5A). Supernatant cytokine analysis confirmed that CD103[−]CD11b⁺

and CD103⁺CD11b⁺ DC_{TME} induce the highest expression of IL-17A and IL-6 in Ova-restricted CD4⁺ T-cell co-cultures (Fig. 4d). We next surveyed the transcriptional regulators in DC-entrained CD4⁺ T cells and similarly discovered that RORγt was expressed most robustly in CD4⁺ T cells that were primed by CD103[−]CD11b⁺ and CD103⁺CD11b⁺ DC_{TME} (Fig. 4e). However, the

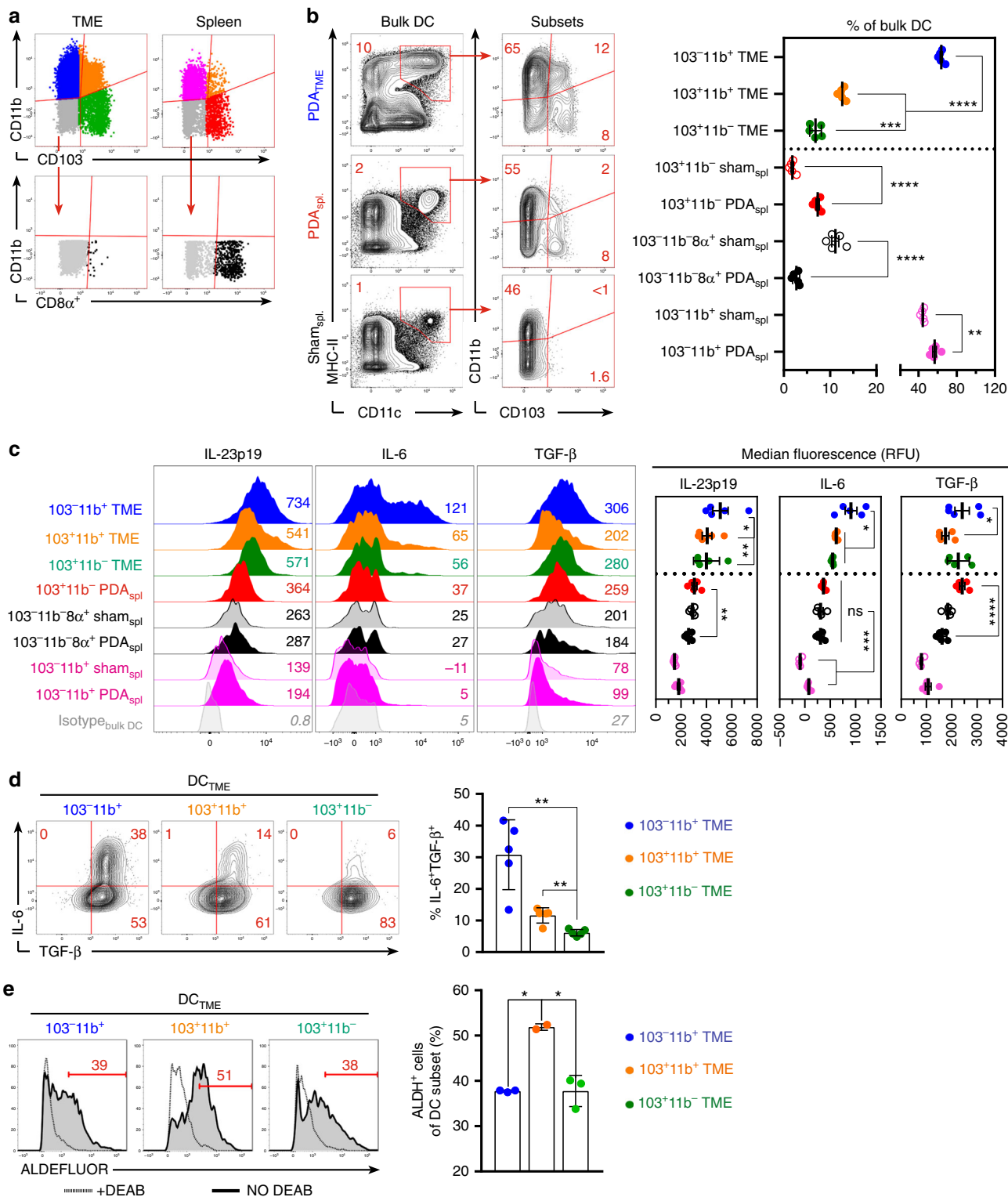
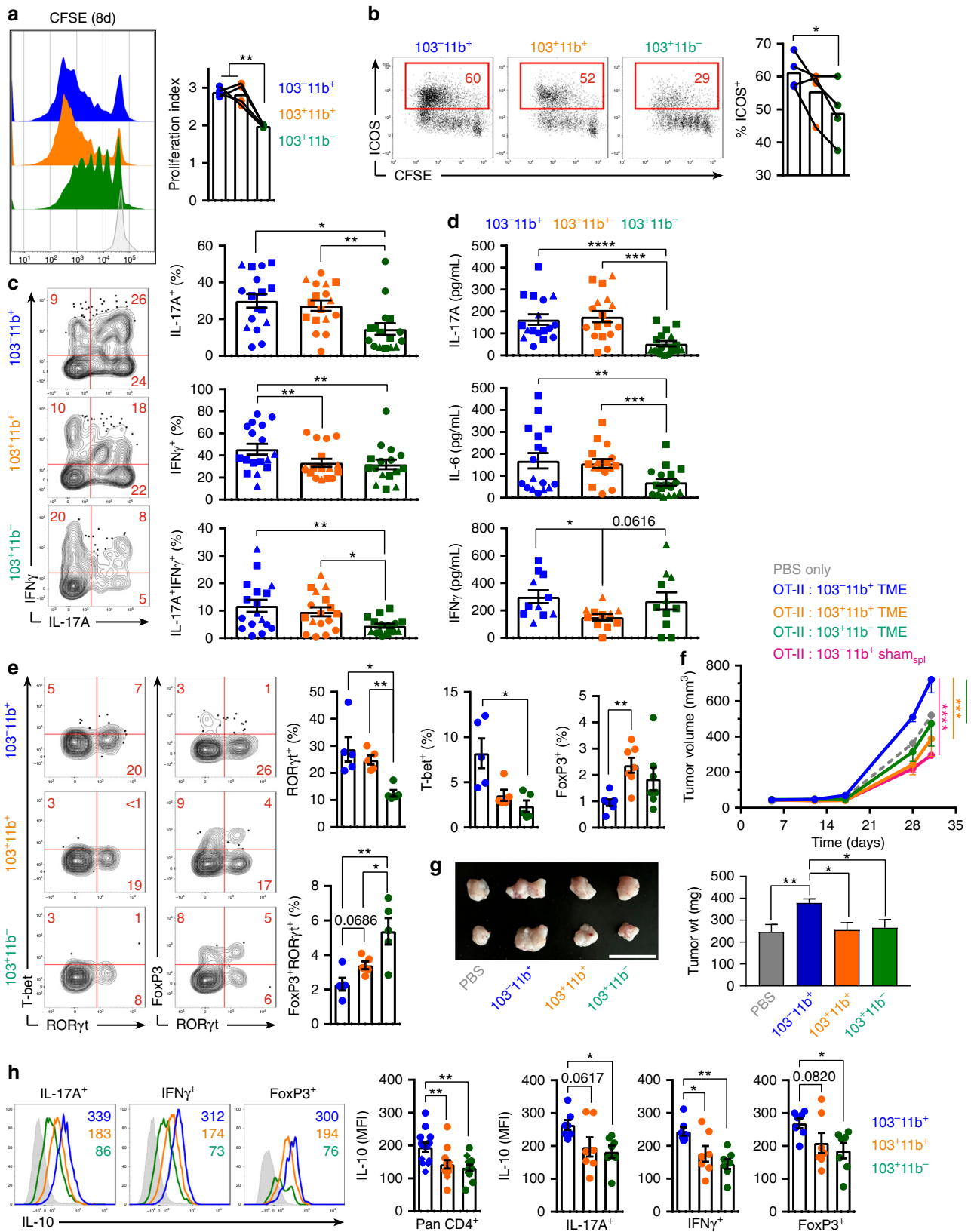


Fig. 3 Specific subsets of PDA_{TME} dendritic cell (DC) exhibit distinct phenotypic properties. **a** The gating strategy for subset analysis of PDA_{TME} and spleen DC based on expression of CD11b, CD103, and CD8 α is depicted. **b** Frequencies of PDA_{TME} and spleen DC subsets based on expression of CD11b, CD103, and CD8 α were analyzed. Representative contour plots and quantitative results are shown. Experiments were repeated >5 times. **c** Histogram plots comparing cytokine expression in distinct DC subsets are shown. Numbers adjacent to histograms represent MFI \div 10. Quantitative data based on MFI are shown. Dotted-line separates PDA_{TME} DC from splenic DC controls. Experiments were repeated three times. **d** The frequency of IL-6 and TGF- β 1 co-expression in PDA_{TME} DC subsets was tested. Representative contour plots and quantitative data are shown. This experiment was repeated three times. **e** Enzymatic activity of ALDH in PDA_{TME} DC subsets was determined by the ALDEFLUOR assay. Gates were determined by respective DEAB controls (dotted histogram) for each individual sample. This experiment was repeated three times (* p < 0.05, ** p < 0.01, *** p < 0.001, **** p < 0.0001, t -test), SEM



CD103⁺CD11b⁺ DC_{TME} induced a slightly higher percentage of FoxP3⁺ T cells, including a distinct population of FoxP3⁺ROR γ t⁺ cells, albeit at low frequency (Fig. 4e). The CD103⁺CD11b⁻ DC_{TME} population also promoted FoxP3⁺ROR γ t⁺ CD4⁺ T-cell differentiation. We questioned whether the FoxP3⁺ CD4⁺ T cells

were able to also produce IL-17, as in previous reports²⁶; however, FoxP3 expression was mutually exclusive of the production of IL-17F (Supplementary Figure 5A) or IL-17A (data not shown). Similarly, expression of IL-17A and FoxP3 in PDA-infiltrating CD4⁺ T cells in situ was also mutually exclusive, as

Fig. 4 CD103⁻CD11b⁺PDA_{TME} dendritic cell (DC) promote the differentiation of suppressive FoxP3^{neg} CD4⁺ T cells. **a–e** Ova_{323–339} peptide-pulsed PDA_{TME} DC subsets were co-cultured with CFSE-labeled Ova-restricted CD4⁺ T cells for 5 days. **a** T-cell proliferation was determined by dilution of CFSE. Representative histograms and quantitative analysis of proliferation indices are shown. **b** T cells were analyzed for co-expression of CFSE and ICOS. Representative and quantitative data are shown. **c** CD4⁺ T cells were analyzed for co-expression of IFN γ and IL-17A. Representative contour plots and quantitative data are shown. Circles, squares, and triangles denote data points from individual mice, pooled from three independent experiments. **d** DC-CD4⁺ T-cell co-culture supernatant were analyzed for expression of IL-17A, IL-6, and IFN γ by cytometric bead array. **e** CD4⁺ T cells were analyzed for co-expression of T-bet/ROR γ t and FoxP3/ROR γ t. Representative contour plots and quantitative data are shown. Experiments were repeated three times with similar results. **f** KPC-derived tumor cells engineered to express Ovalbumin were implanted subcutaneously WT mice admixed with either phosphate-buffered saline (PBS) or Ova-restricted CD4⁺ T cells that had been entrained in vitro using each of the PDA_{TME} DC subsets or CD103⁻CD11b⁺ splenic DC pulsed with Ova_{323–339} peptide. Tumor volume was serially measured ($n = 4–5$ per group). **g** KPC-derived tumor cells were orthotopically implanted in pancreata of WT mice admixed with either PBS or each of the respective PDA_{TME} DC subsets that had been harvested from other pancreatic ductal adenocarcinoma (PDA) tumors. Representative gross images of intra-pancreatic tumors and quantitative data on tumor weight on day 25 are shown. This experiment was repeated twice ($n = 5$ per group; scale bars = 1 μ m). **h** Ova_{323–339} peptide-pulsed PDA_{TME} DC subsets were co-cultured with CFSE-labeled Ova-restricted CD4⁺ T cells for 5 days. T cells stimulated with each respective DC subset were co-stained for IL-10 and either IL-17A, IFN γ , or FoxP3. Expression of IL-10 in pan-CD4⁺ T cells and in IL-17A⁺, IFN γ ⁺, and FoxP3⁺ CD4⁺ T cells was determined. Representative histogram overlays and quantitative data are shown. This experiment was repeated three times (* $p < 0.05$, ** $p < 0.01$, *** $p < 0.001$, **** $p < 0.0001$, t -test), SEM

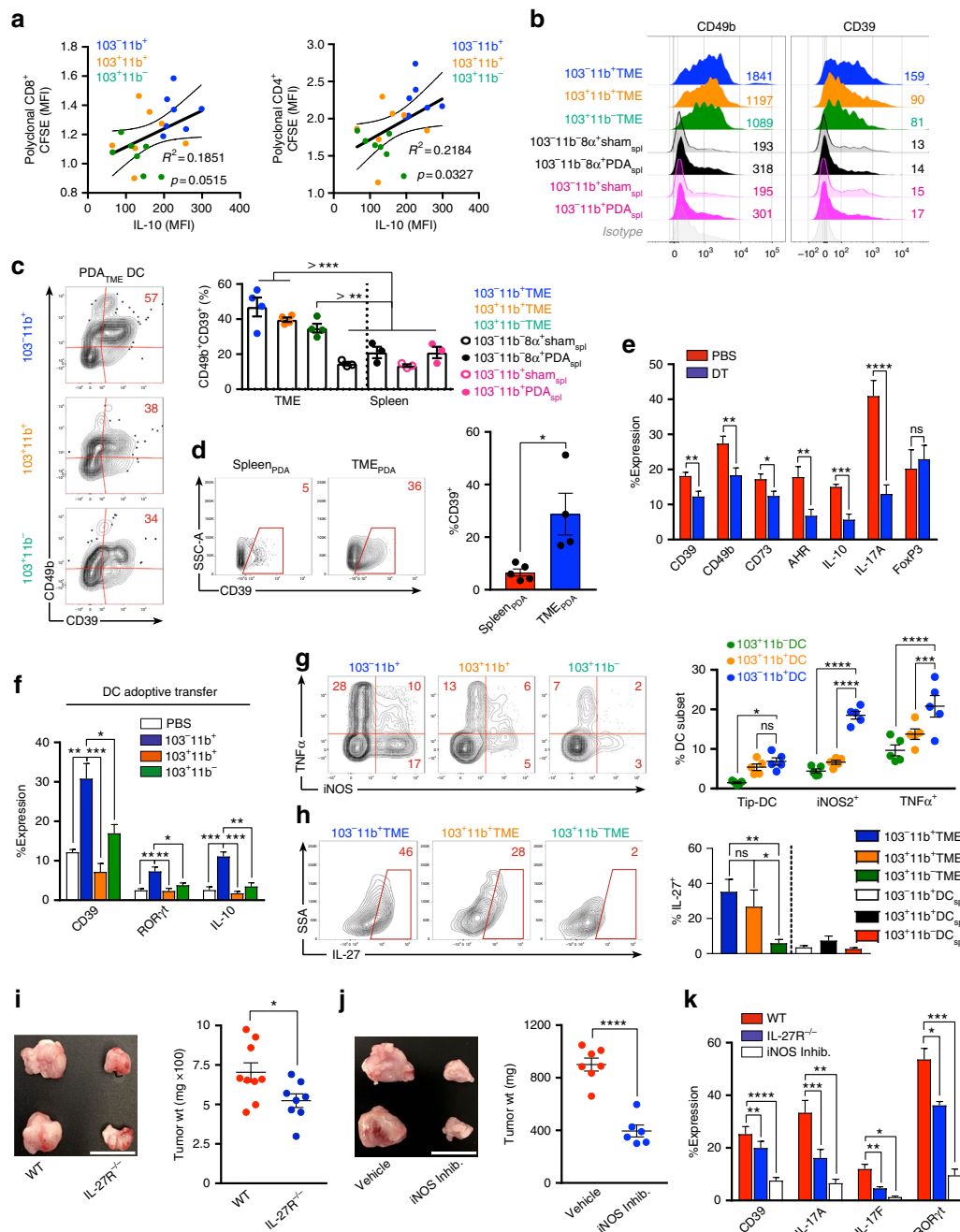
was expression of IFN γ and FoxP3 (Supplementary Figure 5B). These data indicate that IL-17⁺ T cells in PDA are not bona fide FoxP3⁺ peripheral T_{REG}s.

As CD103⁻CD11b⁺ DC_{TME} induced lower FoxP3 expression and higher IFN- γ , we hypothesized that CD4⁺ T cells primed by CD103⁻CD11b⁺ DC_{TME} would promote antitumor immunity and be less suppressive than T_H cells primed by the other PDA_{TME} DC subsets. To test this, we subcutaneously co-injected KPC tumor cells engineered to express ovalbumin with OT-II T cells entrained by the three distinct PDA_{TME} DC subsets. Surprisingly, mice receiving CD103⁻CD11b⁺ DC_{TME}-primed OT-II T cells developed larger tumors than recipients of CD103⁺CD11b⁺ DC_{TME}-primed or CD103⁺CD11b⁻ DC_{TME}-primed T cells (Fig. 4f). Similarly, direct transfer of CD103⁻CD11b⁺ DC_{TME} accelerated PDA growth in vivo whereas other DC_{TME} subsets did not modulate disease progression (Fig. 4g). Furthermore, antigen-restricted CD4⁺ T cells entrained by CD103⁻CD11b⁺ DC_{TME} were inhibitory toward polyclonal CD8⁺ T-cell activation compared with CD4⁺ T cells entrained by other DC_{TME} subsets (Supplementary Figure 5C). Polyclonal CD8⁺ T cells co-cultured with CD4⁺ T cells primed by CD103⁻CD11b⁺ DC_{TME} also exhibited increased cell death (Supplementary Figure 5D). Similarly, the supernatants that were conditioned by CD103⁻CD11b⁺ DC_{TME}-CD4⁺ OTII T-cell co-cultures attenuated the proliferation and activation of polyclonal CD8⁺ and CD4⁺ T cells in vitro to a greater extent than the conditioned media of CD103⁺CD11b⁺ or CD103⁺CD11b⁻ DC_{TME}-CD4⁺ OTII T-cell co-cultures (Supplementary Figure 5E). Moreover, T_H cells primed by CD103⁻CD11b⁺ DC_{TME} expressed greater IL-10 than those primed by other DC_{TME} subsets and this observation of higher IL-10 expression was constant despite gating on IL-17A⁺, IFN γ ⁺, and FoxP3⁺ T cells (Fig. 4h). Further, blockade of IL-10 reversed the inhibitory effects of CD4⁺ T cells entrained by CD103⁻CD11b⁺ DC_{TME} (Supplementary Figure 5F). CD103⁻CD11b⁺ DC_{TME} transfer also failed to accelerate tumor growth in IL-10^{-/-} hosts (Supplementary Figure 5G). Collectively, these data indicate that CD103⁻CD11b⁺ DC_{TME} promote the differentiation of suppressive FoxP3^{neg} CD4⁺ T cells that express high IL-10 as well as substantial IL-17 and IFN- γ .

CD103⁻CD11b⁺ PDA_{TME} DC induce a Tr1-like phenotype in CD4⁺ T cells. Revisiting data from the conditioned media assays, we observed that the frequency of FoxP3⁺ T_{REG}s in co-culture was associated with conditioned media that induced greater proliferation and activation of polyclonal CD4⁺ and CD8⁺ T cells (Supplementary Figure 5H). By contrast, higher IL-10 in CD4⁺ T-cell–PDA_{TME} DC co-cultures was associated with

conditioned media that was more immunosuppressive (Fig. 5a). Tr1 cells are FoxP3^{neg} CD4⁺ T cells, which induce peripheral tolerance through diverse mechanisms^{2,3}. They express IL-10 and IFN γ and have the capacity to produce IL-17. We postulated that CD4⁺ T cells primed by CD103⁻CD11b⁺ DC_{TME} induce characteristic Tr1 cells. Interestingly, all three subsets of PDA_{TME} DC, but not splenic DC, were able to induce expression of the integrin CD49b and the ecto-nucleosidase CD39, each associated with Tr1 cells (Fig. 5b). However, CD103⁻CD11b⁺ DC_{TME} induced the greatest co-expression of CD49b and CD39 (Fig. 5c). Accordingly, we found that a substantial portion of CD4⁺ T cells in the TME, but not the spleen, expressed CD39 in situ (Fig. 5d). Expression of CD49b, CD73, and the aryl hydrocarbon receptor (AHR) were also upregulated in situ in PDA-infiltrating CD4⁺ T cells compared with spleen (Supplementary Figure 5I). Expression of Tr1-associated markers in CD4⁺ T cells in PDA was associated with high co-expression of Granzyme B (Supplementary Figure 5J). Moreover, DC depletion in vivo lowered tumor-infiltrating CD4⁺ T-cell expression of CD39, CD49b, CD73, AHR, IL-17, and IL-10 in PDA suggesting that, besides driving select cytokine expression, DC promote this Tr1-like surface phenotype in PDA-associated CD4⁺ T cells (Fig. 5e). Further, interrogation of the intra-tumoral T-cell phenotype in the DC_{TME} subset adoptive transfer experiments (Fig. 4g) suggested that CD103⁻CD11b⁺ DC_{TME} induce higher CD39, ROR γ t, and IL-10 expression than the other DC_{TME} subsets (Fig. 5f).

DC expression of inducible nitric oxide synthase (iNOS) has been implicated in the differentiation of suppressive FoxP3^{neg} Tr1 cells in inflammatory disease^{27,28}. We found that of the PDA_{TME} DC populations, CD103⁻CD11b⁺ DC_{TME} produced the highest amounts of iNOS, followed by CD103⁺CD11b⁺ DC_{TME} (Fig. 5g). Notably, iNOS expression in DC was largely independent of TNF α production, indicating that PDA_{TME} DC are distinct from the TNF α +iNOS⁺ (Tip)-DC described in the context of infections and allergic diseases^{29,30}. Tumor-associated macrophages also expressed significant iNOS in PDA (Supplementary Figure 5K). Besides iNOS, IL-27 has also been implicated in FoxP3^{neg} Tr1 cellular differentiation³¹. IL-27 was differentially upregulated in CD103⁻CD11b⁺ and CD103⁺CD11b⁺ PDA_{TME} DC subsets (Fig. 5h). Other intra-tumoral leukocyte subsets only produced modest IL-27 in PDA (Supplementary Figure 5L). Moreover, both IL-27R deletion and iNOS inhibition were protective against PDA and, similar to DC depletion, reduced CD4⁺ T-cell expression of CD39, IL-17A, IL-17F, and ROR γ in vivo (Figs. 5i–k). Notably, iNOS inhibition was not tumor protective in absence of DC (Supplementary Figure 5M).



Collectively, these data suggest PDA_{TME} DC promote Tr1-like phenotypes in naive CD4⁺ T cells in an iNOS and IL-27 dependent manner.

High expression of Tr1-associated genes correlates with poor prognosis in PDA patients. To validate our murine findings, we applied our knowledge of CD103⁻CD11b⁺ DC_{TME}-induced T_H cells to patient data from The Cancer Genome Atlas (TCGA). By stratifying PDA patients on the basis of gene expression, we found that the highest quartile of patients expressing each of the “Tr1-related genes”—*CD49b*, *CD73*, and *AHR*—exhibited decreased overall survival (OS) (Fig. 6a). By contrast, expression of T_{REG}-associated genes, including *FoxP3*, *RARα*, and *RARβ*, were not associated with survival differences (Fig. 6a). Given that the expression of *IFNγ* and *IL-17* were each mutually exclusive of *FoxP3* expression (Supplementary Figure 5A and B), we designed

a “validation signature” representing the sum of Tr1-related gene expression subtracted by the sum of T_{REG}-related gene expression. This validation signature was significantly associated with a poor prognosis (Fig. 6a). Stratifying PDA patients by their validation signature scores into high and low quartiles, we discovered that patients in the lowest quartile had a profound OS advantage compared with patients in the highest quartile (Fig. 6b). Furthermore, log-rank (Mantel–Cox) survival curve comparisons between the highest and lowest quartiles displayed greater statistical significance than any gene individually, suggesting that the unique combination of genes in our validation signature may act collectively to drive outcome in PDA patients. This relationship between OS and the validation signature was not observed in other cancers, including breast carcinoma (BRCA), lung adenocarcinoma (LUAD), non-small cell lung cancer (NSLC), and head and neck squamous cell carcinoma (HNSCC) (Supplementary Figure 6A–D). Importantly, the survival phenotype in melanoma

Fig. 5 Pancreatic ductal adenocarcinoma (PDA)-infiltrating dendritic cell (DC) subsets direct distinct CD4⁺ T-cell programs in PDA. **a** CFSE-labeled naive CD8⁺ or CD4⁺ polyclonal T cells isolated from the spleens of WT mice were cultured for 96 h on α CD3e/ α CD28-coated plates in the presence of conditioned media from 8-day OT-II CD4⁺ T cell/PDA_{TME} DC subset co-cultures. Polyclonal T cells were assessed by flow cytometry for CFSE dilution. Each individual well from the OT-II/PDA_{TME} DC subset co-cultures was used to generate conditioned media for a single well of polyclonal CD8⁺ and CD4⁺ T cells. Scatter plots are shown correlating the CFSE dilution of polyclonal T cells to the IL-10 expression of OT-II T cells from the respective OT-II/PDA_{TME} DC subset co-culture used to generate conditioned media. Linear regression was used to determine the best-fit line (solid) and 95% confidence intervals (dotted lines); *p*-values indicate significance of a non-zero slope, determined by an *F*-test. This experiment was repeated twice. **b** Ova₃₂₃₋₃₃₉ peptide-pulsed PDA_{TME} DC subsets and splenic DC subsets were co-cultured with Ova-restricted CD4⁺ T cells at a 1:5 ratio for 5 days. CD4⁺ T-cell expression of CD49b and CD39 were determined compared with isotype control. Representative histograms with MFIs are shown. This experiment was repeated >3 times (*n* = 3–6 mice). **c** Ova₃₂₃₋₃₃₉ peptide-pulsed PDA_{TME} DC subsets and splenic DC subsets were co-cultured with Ova-restricted CD4⁺ T cells at a 1:5 ratio for 5 days. CD4⁺ T-cell co-expression of CD39 and CD49b were determined. Representative contour plots (PDA_{TME} DC) and quantitative data (PDA_{TME} DC, PDA_{Spl} DC, and Sham_{Spl} DC) are shown. Experiments were repeated >3 times (*n* = 3–6 mice). **d** Tumor and spleen were harvested on day 25 from mice bearing orthotopic PDA. Tumor-infiltrating and splenic CD4⁺ T cells were assessed for expression of CD39. Representative and quantitative data are shown. This experiment was repeated >5 times. **e** WT mice were made chimeric using bone marrow from CD11c.DTR mice. Animals were challenged with orthotopic PDA 7 weeks later. On day 12, mice began serial treatment with diphtheria toxin (DT) or phosphate-buffered saline (PBS) before sacrifice and tumor harvest on day 25. Intra-tumoral CD4⁺ T cells were gated on flow cytometry and tested for expression of CD39, CD49b, CD73, AHR, IL-10, IL-17A, and FoxP3. This experiment was repeated >5 times (*n* = 3–10 mice per group). **f** KPC-derived tumor cells were orthotopically implanted in pancreata of WT mice admixed with either PBS or each PDA_{TME} DC subset previously harvested from other PDA tumors. Tumors were then harvested on day 25 and intra-tumoral CD4⁺ T cells were gated on flow cytometry and tested for expression of CD39, ROR γ t, and IL-10. This experiment was repeated twice (*n* = 5 per group). **g** PDA_{TME} DC subsets were tested for co-expression of TNF α and iNOS. Representative contour plots and quantitative data are shown. This experiment was repeated three times. **h** PDA_{TME} and PDA_{Spl} DC subsets were tested for expression of IL-27 compared with isotype control (data not shown). Representative contour plots and quantitative data are shown. This experiment was repeated >3 times (*n* = 5). **i** WT and IL-27R^{-/-} mice were challenged with orthotopic PDA before sacrifice on day 25. Representative pictures of tumors and quantitative data of tumor weight are shown. Each dot represents data from a single mouse. This experiment was repeated three times (Scale bars = 1 μ m). **j** Orthotopic PDA-bearing mice were serially treated with an iNOS inhibitor or vehicle. Tumor volume was measured at 25 days. Representative pictures of tumors and quantitative data of tumor weight are shown. Each dot represents data from a single mouse. This experiment was repeated twice (Scale bars = 1 μ m). **k** WT and IL-27R^{-/-} mice were challenged with orthotopic PDA before sacrifice on day 25. In addition, select cohorts of WT mice were treated with an iNOS inhibitor (*n* = 5 per group). CD4⁺ T-cell expression of CD39, IL-17A, IL-17F, and ROR γ t were determined. This experiment was repeated twice (**p* < 0.05, ***p* < 0.01, ****p* < 0.001, *****p* < 0.0001, *t*-test), SEM

patients was opposite that of PDA patients, with patients in the highest validation signature quartile exhibiting increased OS compared with the lowest quartile (Fig. 6c). This may suggest that suppressive mechanisms blunting antitumor immunity in PDA are distinct from those found in other tumors. Interestingly, in low-grade gliomas (LGGs), a malignancy in which FoxP3⁺ T_{REGS} are not prognostically relevant³², OS based on our validation signature modeled PDA, albeit to a lesser degree of significance (Supplementary Figure 6E).

We next examined the differences in immune-related gene expression in PDA stratified by the Σ Tr1– Σ T_{REG} validation signature score. Consistent with the OS data, the lowest quartile of PDA patients had greater transcriptional expression of *cd3e* and *cd8a*, suggesting the presence of more cytotoxic T cells in the tumor (Fig. 6d). By contrast, melanoma patients scoring high on the validation signature had greater T-cell infiltrates (Fig. 6e). Effective cytotoxic T-cell responses in the TME are mediated by granzymes and perforin, and have been shown to indicate cytolytic activity in tumors across the TCGA database³³. We found that the high validation signature quartile of PDA patients expressed reduced *prf1* compared with the lowest quartile, whereas *gzmb* was similarly expressed in both groups (Fig. 6f). By contrast, melanoma (Fig. 6g) and BRCA (Supplementary Figure 6F) patients in the high validation signature quartile expressed significantly higher cytolytic markers. A similar pattern was seen when grouping all cancers in the TCGA database (Supplementary Figure 6G). Collectively, these data suggest that our Σ Tr1– Σ T_{REG} signature is associated with less cytolytic activity in PDA, but greater cytolytic activity in other cancers.

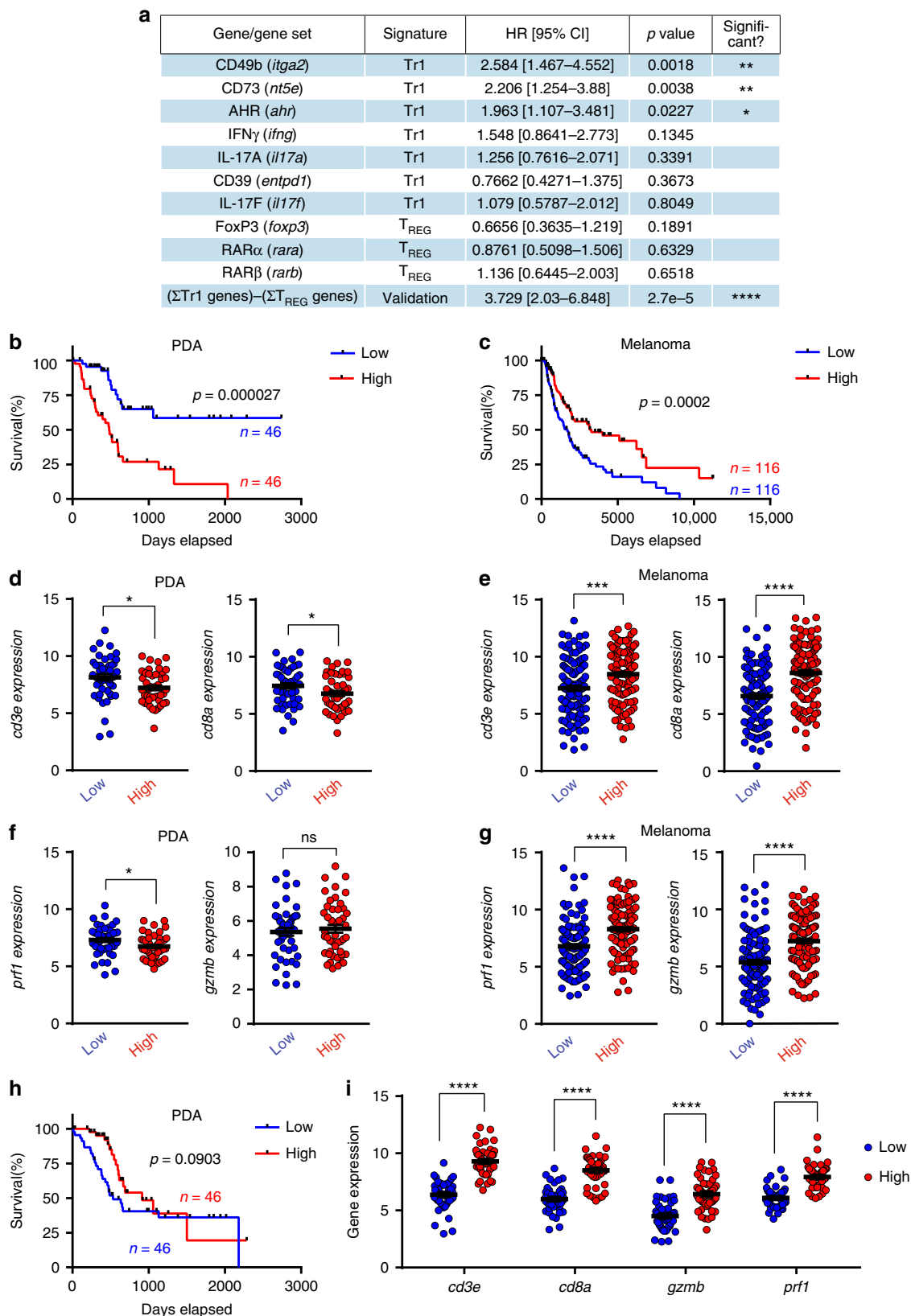
These results made us question the relationship between T_{REG}-associated gene expression and OS in PDA patients. Because Tr1-related genes in the validation signature may also be expressed on T_{REGS}, we created another signature using genes associated exclusively with T_{REGS}. Sorting PDA patients by a simple three-

gene signature representing the sum of *foxp3*, *rara*, and *rarb* expression, we discovered that the highest quartile of scorers conferred a trend towards greater OS than the lowest quartile (Fig. 6h). Moreover, the highest quartile of PDA T_{REG} signature scorers exhibited significantly greater expression of *cd3e*, *cd8a*, *gzmb*, and *prf1* than the PDA patients of the lower quartile (Fig. 6i), suggesting that intra-tumoral T_{REGS} are accompanied by concomitant infiltrates of cytotoxic T cells in PDA patients. Collectively, these analyses validate our preclinical identification of immunosuppressive FoxP3^{neg} CD4⁺ T cells induced by CD103⁻CD11b⁺ PDA_{TME} DC. Furthermore, implications of the differentiation phenotype of these T_H cells are translationally mirrored by the lower OS and diminished intra-tumoral cytolytic activity of PDA patients expressing allied genes.

Discussion

PDA is a devastating diagnosis and carries a grim prognosis. Little progress has been made in the development of new treatments and clinical trials testing checkpoint-based immunotherapies have yielded disappointing results⁵. Nevertheless, there is rationale for pursuing immunotherapeutic manipulation of this disease as immunity or its subversion are strongly associated with disease progression in PDA³⁴. However, the drivers of CD4⁺ T-cell differentiation in the PDA TME and the character of the suppressive T_H phenotype remain incompletely understood.

Tumor-infiltrating CD8⁺ T cells in melanoma are directed toward CTL function by CD103⁺ DC in mice and CD141⁺ DC in humans²⁵. These DC subsets are responsible for trafficking tumor antigen leading to both direct CD8⁺ T-cell stimulation and antigen hand-off to resident myeloid cells. These effects required CCR7. However, unlike melanoma, CD8⁺ T cells are largely irrelevant in PDA as their deletion or depletion does not accelerate oncogenesis^{18,19}. Accordingly, we found that PDA_{TME} DC



do not differentially affect CD8⁺ T-cell activation; conversely, PDA_{TME} DC have distinctive influences on T_H cell programming.

Our cellular ablation experiments using CD11c.DTR mice suggested that, as a bulk population, DC are tumor permissive in PDA in a CD4⁺ T-cell-dependent manner. The CD11c.DTR model has been described as being specific to DC and is the most

widely used method of DC depletion^{35,36}. Nevertheless, this model has limitations relating to both the cellular plasticity of DC and to the recent observation that it is associated with neutrophilia upon DTR administration³⁷. Collectively, we show that PDA_{TME} DC express high T_H1-, T_{REG}-, and T_H17-inducing cytokines and distinctly co-express select inflammatory mediators

Fig. 6 The suppressive program in CD4⁺ T cells blunting antitumor immunity in human pancreatic ductal adenocarcinoma (PDA) is distinct from other human cancers. **a** Data from PDA patients in the TCGA dataset were stratified on the basis of RNAseq gene expression (PolyA⁺ IlluminaHiSeq). Kaplan-Meier survival data comparing the highest and lowest patient quartiles (with the exception of *Il17a* and *Il17f*) are represented as HR with 95% confidence intervals, calculated using the log-rank (Mantel-Cox) method. Statistical comparisons for *Il17a* and *Il17f* represent patients with positive expression of each respective gene versus patients with zero expression. HR values <1 indicate increased OS, whereas values >1 indicate decreased OS for each gene. The developed “validation signature” indicates the gene expression sum of the 7 Tr1-associated genes subtracted by 3 Treg-associated genes ($\Sigma\text{Tr1}-\Sigma\text{T}_{\text{REG}}$). **b** Kaplan-Meier survival curve, plotting the highest (red) and lowest (blue) quartiles of PDA patients from the TCGA database stratified by expression of the $\Sigma\text{Tr1}-\Sigma\text{T}_{\text{REG}}$ signature, with tick marks indicating censored patients. *P*-value was determined using the log-rank (Mantel-Cox) method. **c** Kaplan-Meier survival curve, plotting the highest (red) and lowest (blue) quartiles of melanoma patients from the TCGA dataset, and analyzed with the same methods as in **b**. **d, e** The highest (red) and lowest (blue) quartiles of PDA (**d**) and melanoma (**e**) patients stratified by the $\Sigma\text{Tr1}-\Sigma\text{T}_{\text{REG}}$ validation signature were analyzed for *cd3e* and *cd8a* gene expression; *p*-values were determined by unpaired *t*-test with Welch’s correction. **f, g** Plots represent *prf1* and *gzmB* gene expression in the tumors of patients from the highest (red) and lowest (blue) quartiles of the $\Sigma\text{Tr1}-\Sigma\text{T}_{\text{REG}}$ validation signature from PDA patients (**f**) and melanoma patients (**g**), using RNAseq data from the TCGA database. All dot plots were analyzed with unpaired *t*-tests with Welch’s correction. **h** Kaplan-Meier survival curve, plotting the highest (red) and lowest (blue) quartiles of PDA patients from the TCGA database stratified by expression of three-gene T_{REG} signature, with tick marks indicating censored patients. *P*-value was determined using the log-rank (Mantel-Cox) method. **i** Plots represent *cd3e*, *cd8a*, *gzmB*, and *prf1* gene expression in the tumors of patients from the highest (red) and lowest (blue) quartiles of the three-gene T_{REG} signature from PDA patients. All dot plots were analyzed with unpaired *t*-tests with Welch’s correction (**p* < 0.05, ***p* < 0.01, ****p* < 0.001, *****p* < 0.0001)

including IL-12/IL-23 and IL-6/TGF- β . PDA_{TME} DC capture antigen with marked avidity and are highly mature, including expressing elevated CCR7 and ICOSL. However, PDA_{TME} DC phenotype and functional capacity for driving T_H cell differentiation is dictated by their classification based on CD103 and CD11b expression. Our data suggest that CD103⁻CD11b⁺ DC_{TME} are a major driver of T_H17-inducing cytokines; however, CD103⁺CD11b⁻ DC make equivalent levels of TGF- β to CD103⁻CD11b⁺ DC, and other DC subsets also sufficiently produce additional cytokines that may contribute substantially to Th17 polarization. The CD103⁺CD11b⁻ subset is least abundant and is inefficient at inducing T_H cell proliferation or expression of costimulatory ligands, but induces high FoxP3 expression and FoxP3/ROR γ t co-expression. The CD103⁺CD11b⁺ subset also expresses low levels of inflammatory and regulatory cytokines, but produces high ATRA. This subset also induces high FoxP3⁺ T_{REGS} and has reduced capacity for T_H1 differentiation. However, despite the ostensible tolerogenic T_H phenotype induced by the CD103⁺CD11b⁻ and CD103⁺CD11b⁺ DC populations, CD4⁺ T cells entrained by these DC subsets do not have tumor-promoting or immune-suppressive function based on direct DC adoptive transfer experiments, T_H-cell transfer experiments after DC entrainment, and in vitro conditioned media experiments. By contrast, the CD11b⁺CD103⁻ population, which is the most abundant PDA_{TME} DC subset, have striking tumor-promoting properties based on both direct DC adoptive transfer and transfer of DC-entrained T_H cells. This subset expresses high levels of inflammatory and regulatory cytokines, low ATRA, and induces high CD4⁺ T-cell proliferation and expression of costimulatory molecules. Even more surprising considering their tumor-permissive properties, the CD103⁻CD11b⁺ DC subset induces CD4⁺ T cells to express high T_H1- and T_H17-family cytokines and transcription factors, including a substantial IFN γ ⁺IL17⁺ population, which co-expresses IL-10. In vitro co-culture and in vivo adoptive transfer experiments suggest that the CD103⁻CD11b⁺ subset drives Tr1-associated surface marker expression in CD4⁺ T cells. We found that the immune-suppressive and tumor-promoting effects of these T_H cells are linked, at least in part, to their expression of IL-10.

Tr1 cells have been investigated in allergic and inflammatory contexts and in infectious disease and express high CD39, CD73, CD49b, and AHR³⁸. In these settings, Tr1 cells prevent excessive inflammatory responses, which can lead to autoimmunity, maintaining comparative immune tolerance. However, the role of Tr1 cells in cancer is not well studied. Consistent with our data, the suppressive function of Tr1 cells is mediated in part by their

production of IL-10, which dampens the function of both APCs and antigen-specific effector T cells³. Tr1 cells are by definition FoxP3^{neg} and reportedly produce modest levels of IFN γ ; however, these cells can also express robust IL-17 as we demonstrate. This is particularly notable in PDA as transformed pancreatic ductal epithelial cells upregulate IL-17R and its ligation is mitogenic¹⁴. Tr1 cells can kill both CD8⁺ T cells and myeloid cells through the perforin-granzyme B pathway³⁸. We found that T_H cells in PDA that express the characteristic Tr1 phenotype express high granzyme B. Accordingly, in human PDA low expression of our Tr1-associated validation signature was accompanied by a higher CD8⁺ T-cell infiltrate and a more immunogenic CD8⁺ T-cell profile. Besides targeting CD8⁺ T cells, Tr1 cells can also suppress innate immunity by inhibiting the NLRP3 inflammasome in myeloid cells in an IL-10-dependent mechanism³⁹. Of note, we previously reported that NLRP3 signaling has tolerogenic effects in PDA⁴⁰. However, we do not have direct evidence that Tr1 cells inhibit NLRP3 in PDA. Further, we previously showed that the T-cell mediated suppressive influence on other T-cell subsets can be profound compared with interface between myelomonocytic cells and T cells because of intimate proximity between T cells subsets in the TME¹⁸.

We elucidate biochemical factors governing regulation of T_H phenotype by DC in PDA. Notably, whereas Dectin-1 and TLR2 signaling differentially affected PDA_{TME} DC capacity to secrete cytokines, it did not appreciably alter their capacity for CD4⁺ T-cell differentiation. By contrast, ATRA signaling in PDA_{TME} DC modulated the balance between IL-17-producing T_H cells and T_{REGS}. However, the distinctive Tr1-like T_H differentiation noted in PDA was driven by DC expression of IL-27 and iNOS. We show that all subsets of DC_{TME} produce iNOS; however, CD103⁻CD11b⁺ DC are the highest expressers. Moreover, akin to depleting DC, targeting IL-27 and iNOS were tumor protective in PDA and abrogated many elements of the characteristic CD4⁺ T-cell Tr1-like surface phenotype and cytokine profile in the TME, although mechanistic links to specific DCs subset remains to be defined in vivo. Each of these approaches may be attractive strategies for testing in experimental immunotherapy regimens in PDA. Tr1 cells have been characterized in HNSCC, Hodgkin’s lymphoma, hepatocellular carcinoma (HCC) and colorectal cancer (CRC)⁴¹. Generation of Tr1 cells from naive CD4⁺ T-cell precursors is promoted primarily via immature DC in models of HNSCC, HCC, and liver metastases of CRC^{42,43}. In CRC metastases, Tr1 cells comprise ~30% of the tumor-infiltrating lymphocytes and expressed a diversity of cytokines⁴⁴. Moreover, Tr1 cells in CRC exhibited an

in vitro suppressive activity ~50 times more potent than FoxP3⁺ Tregs. Nevertheless, the clinical impact or consequences of Tr1 cell expansion in cancer is still uncertain. Further, there is no clear direct link between Tr1 cell, the DC subsets we investigated, and patient outcomes in PDA.

Surprisingly, our human data show that FoxP3 expression or upregulation of a three-gene T_{REG} signature was not associated with reduced survival in PDA. This contrasts with a recent report suggesting that targeting T_{REGs} is tumor protective in preclinical models of PDA⁴⁵. Of note, T_{REGs} can have secondary tolerogenic influences in PDA and other malignancies by reciprocally suppressing DC expression of costimulatory ligands^{45,46}. However, our analysis of TCGA data suggests that intra-tumoral T_{REGs} are accompanied by concomitant infiltrates of highly activated cytotoxic T cells in PDA patients, which may account for the absence of a negative prognosis associated with FoxP3 or related gene expression in human disease. Of note, the prognostic value of FoxP3⁺ Tregs in cancer is controversial. A recent meta-analysis of 76 studies encompassing 17 types of cancer, including 15,512 cancer cases, suggested that in aggregate FoxP3⁺ Tregs had a negative effect on survival⁴⁷. However, the prognostic effect varied greatly according to tumor type. High FoxP3⁺ Tregs infiltration was significantly associated with shorter survival in the most solid tumors, including cervical, renal, melanomas, and breast cancers, whereas FoxP3⁺ Tregs were associated with improved survival in colorectal, head and neck, and esophageal cancers.

Immunotherapy has made impressive inroads in clinical therapy for several cancers including melanoma, NSLC, renal cell carcinoma, and HCC. However, PDA has been recalcitrant to checkpoint-based immunotherapy⁵. T-cell scarcity and chemokine-mediated exclusion of T cells from the tumor milieu, reduced T-cell expression of checkpoint receptors, and inability of therapeutic mAbs to physically access PDA-related peri-tumoral fibrosis have each been purported as potential mechanisms of therapeutic resistance in PDA^{21,48,49}. Our current work may further illuminate this conundrum. We found that the suppressive phenotype of CD4⁺ T cells in PDA are distinct compared with other cancers. Specifically, the Σ Tr1- Σ T_{REG} signature is associated with a markedly poor prognosis and immune suppression in PDA, whereas the same signature is associated with tumor protection and antitumor immunity in melanoma. Collectively, our data suggest that, as a result of a distinctive DC-T_H axis, PDA may harbor an immune environment that is different from many other cancers such as melanoma, suggesting that PDA requires a more tailored approach to immunotherapy.

Methods

Animals. C57BL/6J (H-2K_b), Balb/c (H-2K_d), CD11c^{GFP}.DTR, B6N.129P2-*Il27ra^{tm1Mak}/J*, B6.129P2-*Il10^{tm1Cgn}/J*, B6N.129P2-*Il27ra^{tm1Mak}/J*, CD45.1, OT-I, and OT-II mice were purchased from the Jackson Laboratory. KPC mice⁵⁰ were a gift from M. Phillips (New York University). Animals were housed in a clean vivarium and fed standard mouse chow. Bone marrow chimeric animals were created by irradiating mice in a SAARP irradiator (xStrahl Life Sciences). Mice were exposed to two fractions of irradiation (550 rads per dose) interspaced by 6 h, followed by the intravenous (i.v.) bone marrow transfer (10⁷ cells) of nonirradiated donors 12 h after the last dose of radiation. Chimeric mice were used in experiments 6–8 weeks later. To deplete DC in chimeric mice, 1 µg diphtheria toxin was administered intraperitoneal (i.p.); with subsequent doses of 0.2 µg q48h. In select experiments, CD4⁺ (GK1.5) or CD8⁺ T cells (53–6.72; each 150 µg, i.p., q72h; BioXcell) were depleted with neutralizing mAbs as we have previously described¹⁹. To inhibit iNOS, mice were serially treated with 1400 W dihydrochloride (50 µg, q48h, Sigma-Aldrich). Animal procedures were approved by the New York University School of Medicine Institutional Animal Care and Use Committee.

Tumor experiments. The “FC1242” (C57BL/6 background) murine PDA cell line was isolated from the pancreatic tumor of a KPC mouse (*pdx1^{cre/+};KRas^{LSL-G12D}/+;p53^{R172H/+})* as we described previously⁵¹. In select experiments, we utilized FC1242 KPC-derived tumor cells (1 × 10⁶), which we engineered to express OVA

using pCI-neo-cOVA (gift of Maria Castro; Addgene plasmid # 25097) as we described²¹. To establish orthotopic pancreatic lesions in vivo, tumor cells (10⁵) were suspended in phosphate-buffered saline (PBS) with Matrigel (BD) in a 1:1 ratio and were injected into the body of the pancreas via laparotomy. In select experiments, DC (2.5 × 10⁴) were admixed with tumor cells and co-transferred to pancreata of mice. In other experiments, OTII T cells (5 × 10⁴) were admixed with equal numbers of FC1242 and FC1242.Ova tumor cells (2.5 × 10⁴ each) and administered subcutaneously. For our liver metastases model, PDA cells (1 × 10⁶) were administered into the portal venous system via direct splenic injection followed by splenectomy, as we reported⁵².

Cell preparation and flow cytometry. Single-cell suspensions for flow cytometry were prepared as we described previously^{18,19}. Briefly, PDA tumors were placed in cold RPMI-1640 with Collagenase IV (1 mg/mL; Worthington Biochemical), Trypsin inhibitor from soybean (100 µg/mL; Sigma), and DNase I (2 U/mL; Pro-mega) and minced with scissors to sub-millimeter pieces. Tissues were then incubated at 37 °C for 30 min with gentle shaking every 5 min. Specimens were passed through a 70 µm mesh, and centrifuged at 350 g for 5 min. The cell pellet was resuspended in cold PBS with 1% fetal bovine serum. Cell labeling was performed after blocking FcγRIII/II with an anti-CD16/CD32 mAb (eBioscience) by incubating 1 × 10⁶ cells with 1 µg of fluorescence conjugated mAbs directed against murine CD44 (IM7), CD206 (C068C2), CD3 (17A2), CD4 (RM4-5), CD8 (53–6.7), CD39 (Duha5), CD45 (30-F11), CD49b (DX5), CD73 (TY11.8), CD11b (M1/70), CD11c (N418), CD103 (2E7), MHC II (M5/114.15.2), IL-2 (5H4), IL-4 (11B11), IL-6 (MP5-20F3), IL-10 (JES5-16E3), IL-17A (TC11-18H10.1), IL-17F (8F5.1A9), IL-27 (MM27-7B1), CD68 (FA-11), F4/80 (BM8), IFN-γ (XMG1.2), TNFα (MP6-XT22), ICOS (15F9), CD62L (MEL-14), IL-23p19 (fc23cp), IL-12/IL-23p40 (C11.5), IL-12p35 (C15.6), RORγt (AFKJS-9), AHR (4MEJ), TLR-2 (CB225), TGF-β (TW7-16B4), ICOSL (HK5.3), Ms IgG (Poly4053), Rt IgG (Poly4054; all Biolegend), Tbet (eBio4B10), iNOS (CXNFT), IL-13 (eBio13A), FoxP3 (FJK-16s; all ebiosciences), and Dectin-1 (2A11, Abcam). Dead cells were excluded from analysis using zombie yellow (Biolegend). Aldefluor assays were performed using ALDEFUOR kit and DEAB Reagent as per the manufacturer’s protocol (Stemcell Technologies). Intracellular cytokine staining was performed after 3–5 h in vitro stimulation with eBioscience Cell Stimulation Cocktail (plus protein transport inhibitors) using the Foxp3 Transcription Factor Staining Buffer Kit (eBioscience) for cytokines and transcription factors. Flow cytometry was carried out on the LSR-II flow cytometer (BD Biosciences). Data were analyzed using FlowJo v.10.1 (Treestar). DC antigen capture experiments were performed using FITC-Albumin (Sigma) as previously described by us⁵³. Supernatant cytokine levels were measured in a cytometric bead array as per the manufacturer’s protocol (BD Biosciences).

In vivo T-cell proliferation and differentiation assay. The spleens of OT-II and OT-I mice were separately minced with a razor and mashed through a 40 µm strainer to form a single-cell suspension. Erythrocytes were hypotonically lysed with an ammonium chloride-based red blood cell (RBC) lysis buffer and the appropriate T cells were isolated with CD4⁺ T-cell (for OT-II) and CD8⁺ T-cell (for OT-I) isolation kits (Miltenyi). Purified CD4⁺ OT-II and CD8⁺ OT-I T cells were counted, combined at a 1:1 ratio, and stained with 5 µM CellTrace™ CFSE (Life Technologies) for 5 min at room temperature, as previously outlined⁵⁴. CD45.1 recipient mice were injected retro-orbitally (RO) with the Ova-specific T-cell mixture (8 × 10⁶ to 1 × 10⁷) suspended in saline. After 36 h, pancreatic tumors and spleens of tumor-bearing mice were enzymatically dissociated into single-cell suspensions and incubated with both Ova_{257–264} and Ova_{323–339} peptides (10 µg/mL; InvivoGen) at 37 °C for 1.5 h. Cellular suspensions were washed and CD11c⁺ cells were magnetically enriched with ultrapure CD11c microbeads as per the manufacturer’s protocol (Miltenyi). Peptide-pulsed DC (2 × 10⁵) were injected RO into the CD45.1 recipients, which were euthanized 6 days post-DC inoculation. Recipient spleens and mesenteric lymph nodes were harvested for flow cytometric analysis.

In vitro DC-T-cell co-culture assays. Tumor-bearing and control mice were euthanized and pancreatic tumors and spleens were dissociated into single-cell suspensions, pulsed with Ova_{323–339} (10 µg/mL), and magnetically enriched for CD11c⁺ cells, which were then co-cultured at a 1:5 ratio with OT-II T cells (5 × 10⁵) in a 96-well U-bottom plate. Alternatively, antigen-pulsed DC subsets were FAC-sorted on the BD FACSAria™ II using the 100 µm nozzle, centrifuged at 350 × g, and plated onto a 96-well V-bottom plate with 25,000 purified OT-II CD4⁺ T cells at a 1:5 DC:T-cell ratio. After 7–8 days, supernatant was collected and cells were harvested for downstream analysis. T cells were labeled with CFSE in some experiments as per the protocol outlined by Quah et al.⁵⁴. For select experiments, co-cultures occurred in the presence of ATRA (1 µM), LE135 (1 µM, both Sigma), Zymosan depleted (100 µg/ml, InvivoGen), or Pam₂CSK₄ (10 ng/ml, InvivoGen). After 5–8 days, supernatant was collected and cells were harvested for analysis. Allogeneic T-cell proliferation in an MLR was performed as we previously described⁵³.

Conditioned media suppression assay. Polyclonal CD4⁺ and CD8⁺ T cells from the spleens of WT mice were isolated using the CD4⁺ T-cell and CD8⁺ T-cell isolation kits (Miltenyi), respectively, combined at a 1:1 ratio, labeled with CFSE, and 100,000 T cells from this mixture were plated in 50 μ L of complete assay media onto an anti-CD3 ϵ mAb-coated 96-well flat-bottom plate. Next, 50 μ L of the 200 μ L supernatant from the DC subset/OT-II co-cultures was added to the polyclonal T cells and supplemented with 1 μ g/mL of soluble anti-CD28. After 72–84 h, T cells were harvested and assessed by flow cytometry for CFSE dilution and T-cell activation. In select experiments, a neutralizing IL-10 mAb was added (1 μ g/mL, Biolegend).

T-cell adoptive transfer experiments. After 8 days, differentiated OT-II CD4⁺ T cells from the DC subset co-cultures were harvested and fluorescence-activated cell (FAC)-sorted. In total, 5000 purified OT-II T cells were then subcutaneously co-injected with a 1:1 mix of 50,000 FC1242 cells and 50,000 Ova-expressing FC1242 cells. For DC subset co-cultures that did not have extensive OT-II T-cell proliferation (e.g., CD103⁺ DC_{TME}), we pooled OT-II T cells sorted from multiple co-culture wells to be able to harvest enough T cells for injection. Tumor volume was measured by calipers as previously described⁵³. Because of low cell numbers in the subcutaneous tumor cell injections, some tumors did not seed and were excluded from analysis if there was no post-implant growth throughout the 30 days.

TCGA bioinformatics and survival data. RNA sequencing data (polyA⁺ IlluminaHiSeq) representing genome-wide mRNA from patient tumor samples was obtained from individual datasets downloaded from the University of California Santa Cruz Xena browser (UCSC Xena, <http://xena.ucsc.edu>). PDA ($n = 182$), BRCA ($n = 1200$), melanoma (SKCM, $n = 462$), HNSCC ($n = 562$), lung cancer (LUNG (denoted as “NSLC”), $n = 1109$), LUAD ($n = 564$), LGG ($n = 525$), and TCGA PanCancer ($n = 10,264$; data from the Cancer Genome Atlas Research Network; <https://www.cancer.gov/tcga>) datasets were downloaded (08/2017) and filtered to exclude samples with incomplete clinical data (i.e., non-zero, non-“NA”). The validation signature was calculated as the sum of “Tr1 signature” genes subtracted by the sum of “Treg signature” genes as depicted in Fig. 6, and patients from each respective dataset were ranked by validation signature score. Each respective dataset was then divided into quartiles and the highest and lowest quartiles were compared. Kaplan–Meier plots were generated using GraphPad Prism software, and statistical significance of survival curves was determined using the log-rank (Mantel–Cox) test. Hazard ratios of the highest and lowest quartiles of the Pancreatic Adenocarcinoma (PAAD) dataset were reported using the log-rank method, also calculated in GraphPad Prism’s survival analysis statistics. mRNA transcript expression of *CD3 ϵ* , *CD8 α* , *Gzmb*, and *Prf1* was compared between the highest and lowest quartiles of the specified TCGA patients stratified by indicated signatures, and significance was determined by unpaired two-tailed *t*-tests with Welch’s correction. For in vitro assays and mouse tumor experiments, data are presented as mean \pm standard error. Statistical significance was determined by the two-tailed Student’s *t*-test with Welch’s correction; paired and unpaired analysis were conducted where appropriate and indicated in the figure legends.

Ethical statement. All animal experiments were conducted in accordance with a protocol approved by the New York University Institutional Animal Care and Use Committee (IACUC).

Reporting summary. Further information on experimental design is available in the Nature Research Reporting Summary linked to this article.

Data availability

The data that support the findings of this study are available from the corresponding author upon reasonable request.

Received: 4 January 2018 Accepted: 14 February 2019

Published online: 29 March 2019

References

- Hori, S., Nomura, T. & Sakaguchi, S. Control of regulatory T cell development by the transcription factor Foxp3. *Science* **299**, 1057–1061 (2003).
- Le Buanec, H. et al. IFN- α and CD46 stimulation are associated with active lupus and skew natural T regulatory cell differentiation to type 1 regulatory T (Tr1) cells. *Proc. Natl. Acad. Sci. USA* **108**, 18995–19000 (2011).
- Pot, C., Apetoh, L. & Kuchroo, V. K. Type 1 regulatory T cells (Tr1) in autoimmunity. *Semin. Immunol.* **23**, 202–208 (2011).
- Sharma, P. & Allison, J. P. The future of immune checkpoint therapy. *Science* **348**, 56–61 (2015).
- Chen, J., Xiao-Zhong, G. & Qi, X. S. Clinical outcomes of specific immunotherapy in advanced pancreatic cancer: a systematic review and meta-analysis. *J. Immunol. Res.* **2017**, 8282391 (2017).
- Salmon, H. et al. Expansion and activation of CD103(+) dendritic cell progenitors at the tumor site enhances tumor responses to therapeutic PD-L1 and BRAF inhibition. *Immunity* **44**, 924–938 (2016).
- Olive, K. P. et al. Inhibition of Hedgehog signaling enhances delivery of chemotherapy in a mouse model of pancreatic cancer. *Science* **324**, 1457–1461 (2009).
- Plitas, G. & Rudensky, A. Y. Regulatory T cells: differentiation and Function. *Cancer Immunol. Res.* **4**, 721–725 (2016).
- Ruffell, B. et al. Macrophage IL-10 blocks CD8⁺ T cell-dependent responses to chemotherapy by suppressing IL-12 expression in intratumoral dendritic cells. *Cancer Cell* **26**, 623–637 (2014).
- Cua, D. J. et al. Interleukin-23 rather than interleukin-12 is the critical cytokine for autoimmune inflammation of the brain. *Nature* **421**, 744–748 (2003).
- Noack, M. & Miossec, P. Th17 and regulatory T cell balance in autoimmune and inflammatory diseases. *Autoimmun. Rev.* **13**, 668–677 (2014).
- Veldhoen, M. et al. The aryl hydrocarbon receptor links TH17-cell-mediated autoimmunity to environmental toxins. *Nature* **453**, 106–109 (2008).
- Ganguly, D., Haak, S., Sisirak, V. & Reisiz, B. The role of dendritic cells in autoimmunity. *Nat. Rev. Immunol.* **13**, 566–577 (2013).
- McAllister, F. et al. Oncogenic Kras activates a hematopoietic-to-epithelial IL-17 signaling axis in preinvasive pancreatic neoplasia. *Cancer Cell* **25**, 621–637 (2014).
- Miyahara, Y. et al. Generation and regulation of human CD4⁺ IL-17-producing T cells in ovarian cancer. *Proc. Natl. Acad. Sci. USA* **105**, 15505–15510 (2008).
- Wu, S. et al. A human colonic commensal promotes colon tumorigenesis via activation of T helper type 17 T cell responses. *Nat. Med.* **15**, 1016–1022 (2009).
- Yang, S., Fujikado, N., Kolodin, D., Benoist, C. & Mathis, D. Immune tolerance. Regulatory T cells generated early in life play a distinct role in maintaining self-tolerance. *Science* **348**, 589–594 (2015).
- Daley, D. et al. G γ delta T cells support pancreatic oncogenesis by restraining α beta T cell activation. *Cell* **166**, 1485–1499 e1415 (2016).
- Seifert, L. et al. The necrosome promotes pancreatic oncogenesis via CXCL1 and Mincle-induced immune suppression. *Nature* **532**, 245–249 (2016).
- Zhang, Y. et al. CD4⁺ T lymphocyte ablation prevents pancreatic carcinogenesis in mice. *Cancer Immunol. Res.* **2**, 423–435 (2014).
- Daley, D. et al. Dectin 1 activation on macrophages by galectin 9 promotes pancreatic carcinoma and peritumoral immune tolerance. *Nat. Med.* **23**, 556–567 (2017).
- Pushalkar, S. et al. The pancreatic cancer microbiome promotes oncogenesis by induction of innate and adaptive immune suppression. *Cancer Discov.* **8**, 403–416 (2018).
- Dillon, S. et al. Yeast zymosan, a stimulus for TLR2 and dectin-1, induces regulatory antigen-presenting cells and immunological tolerance. *J. Clin. Invest.* **116**, 916–928 (2006).
- Manoharan, I. et al. TLR2-dependent activation of beta-catenin pathway in dendritic cells induces regulatory responses and attenuates autoimmune inflammation. *J. Immunol.* **193**, 4203–4213 (2014).
- Roberts, E. W. et al. Critical role for CD103(+)/CD141(+) dendritic cells bearing CCR7 for tumor antigen trafficking and priming of T cell immunity in melanoma. *Cancer Cell* **30**, 324–336 (2016).
- Voo, K. S. et al. Identification of IL-17-producing FOXP3⁺ regulatory T cells in humans. *Proc. Natl. Acad. Sci. USA* **106**, 4793–4798 (2009).
- Niedbala, W. et al. Nitric oxide-induced regulatory T cells inhibit Th17 but not Th1 cell differentiation and function. *J. Immunol.* **191**, 164–170 (2013).
- Niedbala, W. et al. Nitric oxide induces CD4⁺ CD25⁺ Foxp3 regulatory T cells from CD4⁺ CD25⁺ T cells via p53, IL-2, and OX40. *Proc. Natl. Acad. Sci. USA* **104**, 15478–15483 (2007).
- Bosschaerts, T. et al. Tip-DC development during parasitic infection is regulated by IL-10 and requires CCL2/CCR2, IFN- γ and MyD88 signaling. *PLoS Pathog.* **6**, e1001045 (2010).
- Wilmann-Theis, D. et al. Generation and functional analysis of human TNF- α /iNOS-producing dendritic cells (Tip-DC). *Allergy* **68**, 890–898 (2013).
- Vasanthakumar, A. & Kallies, A. IL-27 paves different roads to Tr1. *Eur. J. Immunol.* **43**, 882–885 (2013).
- Heimberger, A. B. et al. Incidence and prognostic impact of FoxP3⁺ regulatory T cells in human gliomas. *Clin. Cancer Res.* **14**, 5166–5172 (2008).
- Rooney, M. S., Shukla, S. A., Wu, C. J., Getz, G. & Hachohen, N. Molecular and genetic properties of tumors associated with local immune cytolytic activity. *Cell* **160**, 48–61 (2015).
- Vonderheide, R. H. & Bayne, L. J. Inflammatory networks and immune surveillance of pancreatic carcinoma. *Curr. Opin. Immunol.* **25**, 200–205 (2013).
- Bennett, C. L. & Clausen, B. E. DC ablation in mice: promises, pitfalls, and challenges. *Trends Immunol.* **28**, 525–531 (2007).

36. Jung, S. et al. In vivo depletion of CD11c+ dendritic cells abrogates priming of CD8+ T cells by exogenous cell-associated antigens. *Immunity* **17**, 211–220 (2002).
37. van Blijswijk, J., Schraml, B. U. & Reis e Sousa, C. Advantages and limitations of mouse models to deplete dendritic cells. *Eur. J. Immunol.* **43**, 22–26 (2013).
38. Chihara, N., Madi, A., Karwacz, K., Awasthi, A. & Kuchroo, V. K. Differentiation and characterization of Tr1 cells. *Curr. Protoc. Immunol.* **113**, 3 27 21–23 27 10 (2016).
39. Yao, Y. et al. Tr1 Cells, but not Foxp3+ Regulatory T cells, suppress NLRP3 inflammasome activation via an IL-10-dependent mechanism. *J. Immunol.* **195**, 488–497 (2015).
40. Daley, D. et al. NLRP3 signaling drives macrophage-induced adaptive immune suppression in pancreatic carcinoma. *J. Exp. Med.* **214**, 1711–1724 (2017).
41. Chaudhary, B. & Elkord, E. Regulatory T cells in the tumor microenvironment and cancer progression: role and therapeutic targeting. *Vaccines (Basel)* **4**, 28 (2016).
42. Bergmann, C. et al. T regulatory type 1 cells in squamous cell carcinoma of the head and neck: mechanisms of suppression and expansion in advanced disease. *Clin. Cancer Res* **14**, 3706–3715 (2008).
43. Pedroza-Gonzalez, A. et al. Tumor-infiltrating plasmacytoid dendritic cells promote immunosuppression by Tr1 cells in human liver tumors. *Oncoimmunology* **4**, e1008355 (2015).
44. Scurr, M. et al. Highly prevalent colorectal cancer-infiltrating LAP(+) Foxp3(–) T cells exhibit more potent immunosuppressive activity than Foxp3(+) regulatory T cells. *Mucosal Immunol.* **7**, 428–439 (2014).
45. Jang, J. E. et al. Crosstalk between regulatory T cells and tumor-associated dendritic cells negates anti-tumor immunity in pancreatic cancer. *Cell Rep.* **20**, 558–571 (2017).
46. Onishi, Y., Fehervari, Z., Yamaguchi, T. & Sakaguchi, S. Foxp3+ natural regulatory T cells preferentially form aggregates on dendritic cells in vitro and actively inhibit their maturation. *Proc. Natl. Acad. Sci. USA* **105**, 10113–10118 (2008).
47. Shang, B., Liu, Y., Jiang, S. J. & Liu, Y. Prognostic value of tumor-infiltrating FoxP3+ regulatory T cells in cancers: a systematic review and meta-analysis. *Sci. Rep.* **5**, 15179 (2015).
48. Feig, C. et al. Targeting CXCL12 from FAP-expressing carcinoma-associated fibroblasts synergizes with anti-PD-L1 immunotherapy in pancreatic cancer. *Proc. Natl. Acad. Sci. USA* **110**, 20212–20217 (2013).
49. Provenzano, P. P. et al. Enzymatic targeting of the stroma ablates physical barriers to treatment of pancreatic ductal adenocarcinoma. *Cancer Cell* **21**, 418–429 (2012).
50. Hingorani, S. R. et al. Trp53R172H and KrasG12D cooperate to promote chromosomal instability and widely metastatic pancreatic ductal adenocarcinoma in mice. *Cancer Cell* **7**, 469–483 (2005).
51. Zambirinis, C. P. et al. TLR9 ligation in pancreatic stellate cells promotes tumorigenesis. *J. Exp. Med.* **212**, 2077–2094 (2015).
52. Miller, G., Lahrs, S., Shah, A. B. & DeMatteo, R. P. Optimization of dendritic cell maturation and gene transfer by recombinant adenovirus. *Cancer Immunol. Immunother.* **52**, 347–358 (2003).
53. Miller, G., Lahrs, S., Pillarisetty, V. G., Shah, A. B. & DeMatteo, R. P. Adenovirus infection enhances dendritic cell immunostimulatory properties and induces natural killer and T-cell-mediated tumor protection. *Cancer Res* **62**, 5260–5266 (2002).
54. Quah, B. J., Warren, H. S. & Parish, C. R. Monitoring lymphocyte proliferation in vitro and in vivo with the intracellular fluorescent dye carboxyfluorescein diacetate succinimidyl ester. *Nat. Protoc.* **2**, 2049–2056 (2007).

Acknowledgements

Cell sorting/flow cytometry technologies were provided by NYU Langone's Cytometry and Cell Sorting Laboratory, which is supported in part by grant P30CA016087 from the National Institutes of Health/National Cancer Institute. The results published here are in part based upon data generated by the TCGA Research Network: <https://www.cancer.gov/tcga>.

Author contributions

R.M.B., B.D.: manuscript preparation, in vivo and in vitro experiments, designed, supervised, data analysis, and study interpretation, co-first authors; R.C.C.: in vitro experiments; K.B.L., N.M., C.B., and S.A.: in vivo experiments and manuscript/figure preparation; Z.S., J.W., R.D.S., M.F.C., J.K., B.S., H.A., D.L., I.G., J.G., W.W., M.H., A.T.-H., J.L., E.K., J.A.K.R., A.M., M.L., and G.S.: in vivo experiments, data analysis, manuscript review; J.P. and P.L.: data analysis and critical review; G.M.: conceived, designed, supervised, analyzed and interpreted the study and provided critical review, senior author, lead contact.

Additional information

Supplementary Information accompanies this paper at <https://doi.org/10.1038/s41467-019-09416-2>.

Competing interests: G.M. has research agreements with GSK, Pfizer, and Puretech Health. The remaining authors declare no competing interests.

Reprints and permission information is available online at <http://npg.nature.com/reprintsandpermissions/>

Journal peer review information: *Nature Communications* thanks the anonymous reviewers for their contribution to the peer review of this work.

Publisher's note: Springer Nature remains neutral with regard to jurisdictional claims in published maps and institutional affiliations.



Open Access This article is licensed under a Creative Commons Attribution 4.0 International License, which permits use, sharing, adaptation, distribution and reproduction in any medium or format, as long as you give appropriate credit to the original author(s) and the source, provide a link to the Creative Commons license, and indicate if changes were made. The images or other third party material in this article are included in the article's Creative Commons license, unless indicated otherwise in a credit line to the material. If material is not included in the article's Creative Commons license and your intended use is not permitted by statutory regulation or exceeds the permitted use, you will need to obtain permission directly from the copyright holder. To view a copy of this license, visit <http://creativecommons.org/licenses/by/4.0/>.

© The Author(s) 2019